Journal of Plant Physiology 265 (2021) 153505

Contents lists available at ScienceDirect

Journal of Plant Physiology

journal homepage: www.elsevier.com/locate/jplph

The metabolic environment of the developing embryo: A multidisciplinary approach on oilseed rapeseed

Hardy Rolletschek [a], Simon Mayer [a], Berin Boughton [b], Steffen Wagner [a], Stefan Ortleb [a], Christina Kiel [a], Ute Roessner [c], Ljudmilla Borisjuk [a,*]

[a] Leibniz-Institut für Pflanzengenetik und Kulturpflanzenforschung (IPK), Corrensstrasse 3, 06466, Seeland-Gatersleben, Germany
[b] Australian National Phenome Centre, Murdoch University, Western Australia, 6150, Australia
[c] School of BioSciences, The University of Melbourne, Victoria, 3010, Australia

ARTICLE INFO

Keywords:
Brassica napus
Endosperm
Embryo
MRI
CSI
MALDI-Imaging
Isotope labelling
Seed development

ABSTRACT

Brassicaceae seeds consist of three genetically distinct structures: the embryo, endosperm and seed coat, all of which are involved in assimilate allocation during seed development. The complexity of their metabolic interrelations remains unresolved to date. In the present study, we apply state-of-the-art imaging and analytical approaches to assess the metabolic environment of the *Brassica napus* embryo. Nuclear magnetic resonance imaging (MRI) provided volumetric data on the living embryo and endosperm, revealing how the endosperm envelops the embryo, determining endosperm's priority in assimilate uptake from the seed coat during early development. MRI analysis showed higher levels of sugars in the peripheral endosperm facing the seed coat, but a lower sugar content within the central vacuole and the region surrounding the embryo. Feeding intact siliques with ^{13}C-labeled sucrose allowed tracing of the post-phloem route of sucrose transfer within the seed at the heart stage of embryogenesis, by means of mass spectrometry imaging. Quantification of over 70 organic and inorganic compounds in the endosperm revealed shifts in their abundance over different stages of development, while sugars and potassium were the main determinants of osmolality throughout these stages. Our multidisciplinary approach allows access to the hidden aspects of endosperm metabolism, a task which remains unattainable for the small-seeded model plant *Arabidopsis thaliana*.

1. Introduction

Crops belonging to the *Brassicaceae* family, such as oilseed rape (*Brassica napus*), exhibit high phylogenetic similarity to the model plant *Arabidopsis thaliana*, on which extensive investigations have provided valuable information and molecular tools (Provart et al., 2016). While *Arabidopsis* develops, reproduces and responds to stress and disease similarly to crop plants, the latter are often much more complex and difficult to characterize. There is a need to critically evaluate observations generated to date, and to test hypotheses and feasibility of models on real crops.

Oilseed rapeseed is the most important source of vegetable oil in Europe, and has moved *B. napus* into the focus of scientific research during the last decades (Chalhoub et al., 2014; Clarke et al., 2016; Borisjuk et al., 2013a,b; Rolletschek et al., 2020). The seeds of *B. napus* are larger than those of *Arabidopsis* and are thus easily accessible for biochemical and *in vivo* studies. The developing seeds of both plants represent complex metabolic systems, involving at least a tripartite interaction among the testa (integuments or seed coat), endosperm and embryo. These three components form a system of autonomous, yet interacting organs, each regulated by their own genetic program (Lau et al., 2012). The application of breakthrough technologies and novel molecular approaches has revealed the highly complex relationship between the developing embryo and its surrounding tissues. In *A. thaliana* and *B. napus*, rapid growth of the testa and endosperm at early development is critical in seed size determination (Garcia et al., 2005; Li and Berger, 2012; Lafon-Placette and Köhler, 2014; Ingram, 2020). During further development, the embryo enlarges, compresses the endosperm and eventually fills out the seed interior, constituting the main storage depot for oils and proteins. Considerable cellular,

* Corresponding author. Leibniz-Institut für Pflanzengenetik und Kulturpflanzenforschung (IPK), Corrensstrasse 3, 06466, Gatersleben, Germany.
E-mail addresses: rollet@ipk-gatersleben.de (H. Rolletschek), mayer@ipk-gatersleben.de (S. Mayer), Berin.Boughton@murdoch.edu.au (B. Boughton), wagner@ipk-gatersleben.de (S. Wagner), ortleb@ipk-gatersleben.de (S. Ortleb), koenig.christina@freenet.de (C. Kiel), u.roessner@unimelb.edu.au (U. Roessner), borysyuk@ipk-gatersleben.de (L. Borisjuk).

https://doi.org/10.1016/j.jplph.2021.153505
Received 28 May 2021; Received in revised form 9 August 2021; Accepted 18 August 2021
Available online 28 August 2021

molecular and biochemical shifts accompany these developmental events, orchestrated by transcription factors and hormones (Baud et al., 2016; Wu et al., 2020).

From a physiological point of view, the developing seed is a net importer of photosynthetic products. As any other 'sink' organ, it receives nutrients via the phloem, though a peculiarity is noted in these plants compared to tubers or fruits: the phloem strands end in the maternal testa surrounding the filial sink organs. Inherent to this architecture is that both filial organs are symplastically isolated from the mother plant. Therefore, apoplastic transport is an essential and regulatory element in post-phloem assimilate allocation within a developing seed (Patrick and Offler, 2001). Indeed, a sophisticated cascade of transporters involved in phloem unloading, nutrient release into the endosperm and uptake into the embryo forms the 'yin and yang' in assimilate partitioning and eventual seed formation (Baud et al., 2005; Melkus et al., 2009; Chen et al., 2015). The suspensor can also participate in some transport processes, but only at very early stage (Kawashima and Goldberg, 2010). There is much potential in the manipulation of this machinery for the purpose of crop improvement (Fernie et al., 2020).

Physical restrictions (space and light) from the seed coat have been shown to affect both endosperm and embryo development (Borisjuk et al., 2013a,b; Fourquin et al., 2016; Rolletschek et al., 2021). The hormonal, metabolic and other signals derived from the vascular system (mother plant) are not purely nor instantly transmitted to the embryo, but underlie modulation within the testa and endosperm. Hence, the endosperm is not merely a neighboring structure of the embryo within the seed coat, but is a site of metabolic and hormonal activity (Figueiredo and Köhler, 2018). The metabolic environment experienced by the developing embryo is largely defined by the endosperm, its biochemical composition and physical constraints. Accordingly, an in-depth investigation of the endospermal matter that directly surrounds and transmits to the embryo is required to fully understand embryonic growth dynamics, the related sink strength and, ultimately, seed yield as a major agronomic trait. The study of the living endosperm is difficult for conventional microscopy for many reasons. First, because the endosperm is localized inside the seed coat, which is a bulky multilayered structure, which does not allow direct microscopic observation; second, any damage of seed coat or endosperm could disturb distribution of metabolites and interrupt embryogenesis; third, endosperm itself is a heterogenic structure, with dynamically altering size and state. Thus, a noninvasive approach appears most appropriate for investigation of endosperm.

Nuclear Magnetic Resonance (NMR) is a powerful technical platform based on the use of magnetic fields, magnetic field gradients, and radio waves to generate images of living organisms (for technical details, see Bernstein et al., 2004; Borisjuk et al., 2012). Traits of interest can be non-invasively analyzed at many different levels – inner structure, biochemistry and dynamic - and this makes the uniqueness of Magnetic Resonance Imaging (MRI). MRI technology is widely used in medical diagnostic, but much less in plant science (Borisjuk et al., 2012). Some dedicated MRI applications have been developed specifically for seeds, enabling the three-dimensional modeling of anatomy and metabolite distribution for the comparative analysis of transgenic plants (Radchuk et al., 2018; Rolletschek et al., 2020), mutants (Meitzel et al., 2021), distant crosses (Tikhenko et al., 2020) and evaluation of environmental effects (Rolletschek et al., 2015, 2021). Using MRI, it became possible to visualize the 3D distribution of lipids (Borisjuk et al., 2013a,b; Woodfield et al., 2017) and to monitor dynamic processes, as for example germination (Munz et al., 2017) and sugar allocation (Melkus et al., 2011; Fuchs et al., 2015; Radchuk et al., 2021).

Herein, we aimed to define the metabolic environment of the developing embryo of *B. napus*. At the molecular level, the transcriptome and proteome machinery of *B. napus* endosperm has been described previously (Lorenz et al., 2014; Ziegler et al., 2019; Khan et al., 2020). We therefore focused on the biochemical level, with an analysis of nutrient transfer toward the embryo, for which limited information is currently available (Hill et al., 2003; Morley-Smith et al., 2008). For this purpose, we initially applied non-invasive MRI to non-destructively inspect certain structural features in early endosperm and embryo development. MR-spectroscopy allowed us to visualize *in vivo* gradients of sugar distribution within the endosperm. We then performed a quantitative analysis of the main constituents of the endosperm, formed by assimilates, metabolic intermediates and inorganic ions. Finally, we used an *in vitro* silique culture system to quantitatively assess the assimilate partitioning among seed organs, by means of isotopically labeled substrates. By applying mass spectrometry imaging (MSI), we could spatially resolve the transfer of (labeled) sucrose from the testa toward the embryo, via the endosperm. Our multifaceted approach provides a rich dataset, valuable not only for the crop species *B. napus*, but, by implication, also for its close relative *A. thaliana*, for which comparable datasets are not available, primarily due to technical limitations (seed size).

2. Results

2.1. Magnetic resonance imaging displayed the three-dimensional morphology of living seed

To explore the spatial *in vivo* arrangement of seeds inside siliques, we analyzed intact silique using MRI applying frequency-selective excitation pulses at the water and lipid frequencies. This strategy enabled us to gain structural elements of the seed and to visualize lipid deposition, both with high resolution. Computer modeling facilitated visual representation of data obtained from the MRI system and allowed to demonstrate deposition of lipid in the morphological context (Fig. 1). The seed is attached to silique via the funiculus (Fig. 1A), which is a tubular structure specialized for mechanical support and solute translocation between silique and seed (Chan and Belmont, 2013). The vascular bundle is well seen in central part of funiculus (Fig. 1B), and connects the seed to the vascular system of silique and thus vascular network of the entire plant. Vasculature is terminated at specific position in the seed coat (chalazal region). The embryo does not have any contact to the vasculature and is enclosed by the seed coat and endosperm. The central part of seed interior is occupied by a large vacuole (Fig. 1B and Supplemental Movie 1).

MRI clearly showed that accumulation of lipid in the endosperm did not occur within the chalazal region of the seed (Fig. 1C). Based on observations in *Arabidopsis* (Keith et al., 1994) and *Brassica* (Groot and van Caeseele, 1993), lipid accumulation in endosperm is restricted to the endosperm epidermis (aleurone) which cells also develops thick multilayered walls. Later in development, it generates cuticular compounds consisting of soluble and polymerized lipids (De Giorgi et al., 2015). Finally, the aleurone layer represents an isolating barrier, which encloses the embryo and influences seed dormancy/germination (Penfield, 2017; Munz et al., 2017). The lack of an isolating barriers (like lipid layer) in close proximity to the vascular tissue in developing seed (as shown here) might indicate a facilitated exchange of solutes (and gases) within this region (Molina et al., 2008).

We conclude that MRI clearly visualised the architecture of the seed interior and exact positioning of seed organs with respect to vascular vessels in the living seed and across the intact silique. The 3D arrangement of endosperm clearly showed the absence of a lipid barrier within a certain area of the endosperm, which is faced to the chalazae and vascular margin. This is in accord with previous studies, which identified a main phloem-unloading domain at the end of the funicular phloem (Stadler et al., 2005; Werner et al., 2011).

2.2. Volumetric analysis of the living endosperm and its relation to the embryo

MRI data were further used to generate three-dimensional (3-D)

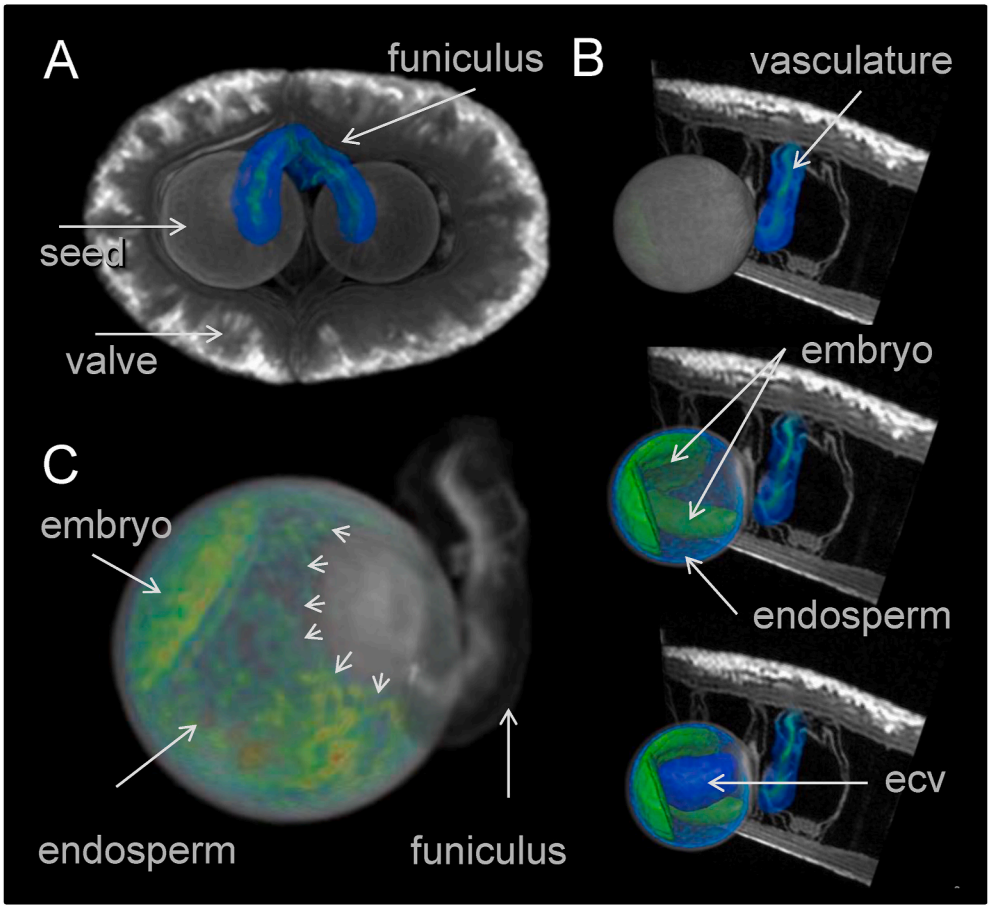

Fig. 1. Modeling of three-dimensional arrangement of living seed inside of silique in oilseed rape based on magnetic resonance imaging. (A) Non-invasive analysis of seed inside of silique; funiculus is highlighted in blue; (B) fragments of the 3-D model of silique and seed displaying the internal arrangement of seed: longitudinal section though the silique; endosperm is semitransparent to display the positioning of embryo. See also Supplemental Movie 1. (C) Deposition of lipid in embryo and endosperm by high resolution lipid imaging in living seed at 24 DAF; the border of lipid-enriched endosperm is arrowed. Abbreviations: ecv – endosperm central vacuole.

models of the seed at distinct stages (Fig. 2A–D and Supplemental Movie 2), providing information on the shape and size of the living seed itself as well as its organs during the time frame from 12 to 30 days after flowering (DAF). The orientation of embryos (highlighted in yellow; Fig. 2A) inside of individual seeds and the spatial arrangement of the lipid accumulation in embryos and endosperm (in respect to funiculus and vascular bundle) was nearly identical among seeds (Supplemental Movie 2). The virtual cross sections displayed details of the lipid deposit in the embryo radicle, both cotyledons and aleurone of endosperm (Fig. 2B). While the endosperm central vacuole remained its liquid state, a large portion of endosperm was cellularized and enveloped the embryo radicle and outer cotyledons (Fig. 2C,F). In order to visualize the dramatic alterations occurring inside the seed during its growth, we measured the volume of endosperm, embryo and seed coat and quantified their ratio across the embryogenesis (Fig. 2D). According to MRI-based volumetric data, the seed size increased continuously from 5.3 to 7.8 mm^3 during the developmental period analyzed (Fig. 2E). The changes in the seed coat size were minor compared with the marked transitions observed in the seed interior. Based on volume, the endosperm (including the central vacuole) was the dominant compartment at stages a–c, contributing to ~70% of the seed volume (Fig. 2E). Our 3-D seed models indicate that the endosperm completely enveloped the embryo, which remained small up to stage c, but exhibited significant growth thereafter. This included the preferential growth of the two cotyledons, leading to a large increase in the embryo surface area (Fig. 2G), an aspect likely relevant to assimilate uptake into the embryo. The thickness of the cotyledons was seen to increase continuously, resulting in a ~60-fold increase in the embryo volume (stages a–d: 0.08–4.9 mm^3).

2.3. Non-invasive MR spectroscopy for the visualization of sugar gradients in the endosperm

We subsequently investigated the biochemical features of the intact endosperm of *B. napus*, using MR spectroscopy and imaging. The slice selective chemical shift imaging (CSI) method was applied in spin-echo mode. The measurement protocol (Melkus et al., 2009) was experimentally optimized to reach sufficient spatial and spectroscopic resolution in a short measurement time. A virtual tissue slice was excised from the seed (Fig. 3A–E) so that the seed coat, embryo and endosperm were all discernible in the image. With the MRI procedure used in the present analysis, the distribution of sugars, water, and lipids was visible within the interior of ~2-mm seeds. The differences in specific signal distribution were detected with 165 × 165 μm^2 in-plane resolution with a measurement time of ~40 min.

MR spectroscopy detected a gradient in sugar distribution (Fig. 3B). Low levels corresponded to the central vacuole, whereas higher signals were observed near the periphery of the endosperm (faced to the seed coat), and levels were lowest in the area of the embryo and its immediate surroundings. The signals characteristic for lipids (Fig. 3D) were strongly detected in the embryo axis (Fig. 3D), but only traces of lipid were detected at this early stage in the outermost endosperm layer (not shown). The highest water signal was colocalized with the central part of seed (central vacuole) (Fig. 3E). In the area of the embryo and seed coat, a weaker water signal was observed, and in the region of the cellularized endosperm, it was slightly lower than for the central vacuole.

To conclude, MRI was capable to *in vivo* access local metabolic features of the seed interior, which emerges from cellular processes common to embryo, endosperm and seed coat. Compartmentation and gradients of water, sucrose and lipids in the living seed were visualised with high spatial resolution. The most notable finding of the high-

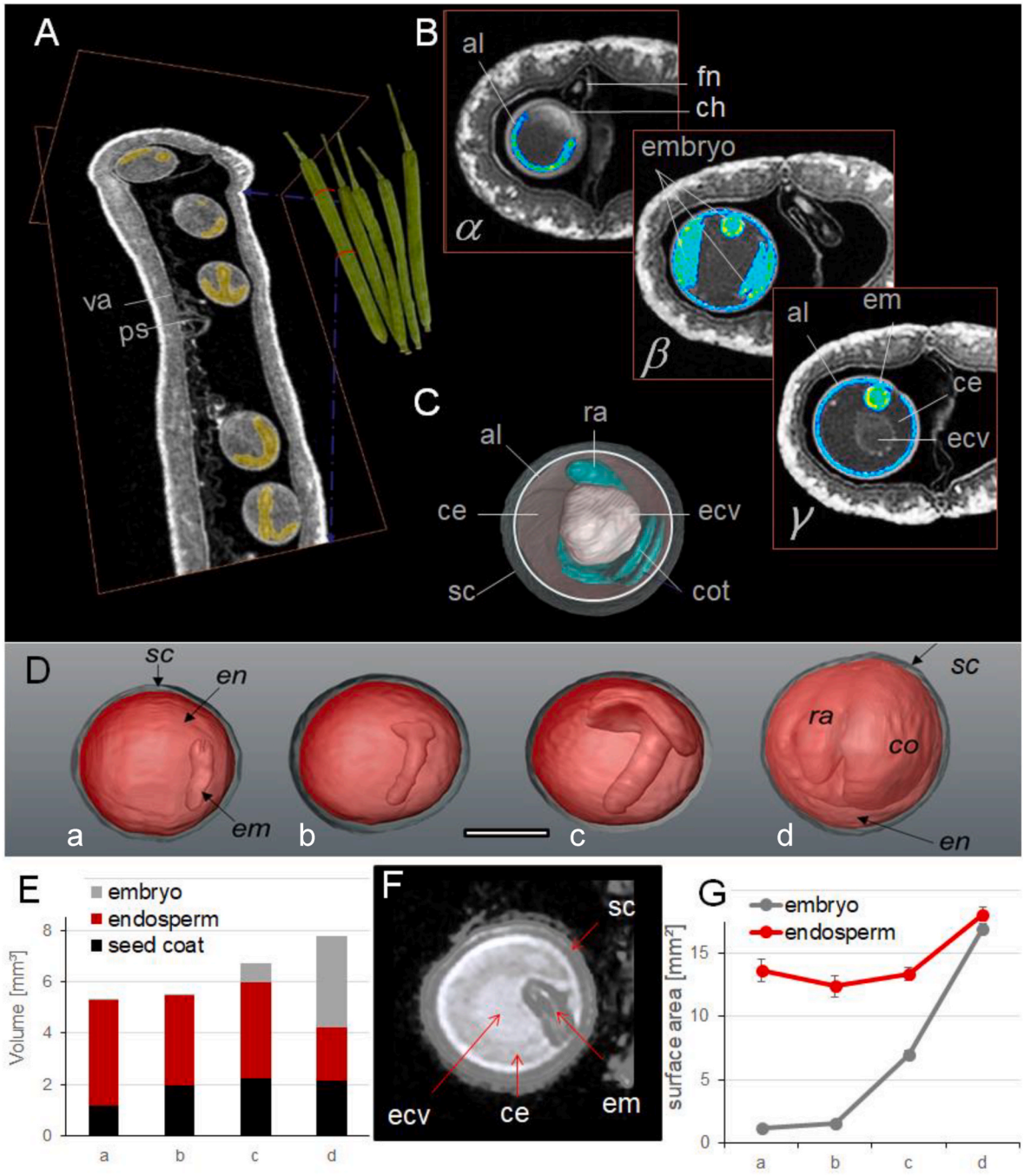

Fig. 2. Volumetric analysis of developing oilseed rapeseed based on magnetic resonance imaging. (A) Non-invasive visualization of seed and embryo inside of silique; note distinct orientation of embryos highlighted in yellow (18 DAF). (B) Virtual cross sections displaying spatial arrangement of seed components at mid cotyledon stage of development (21 DAF); there distinct cross-sections are shown; see also Supplemental Movie 2. (C) 3-D-seed model showing all individual components. (D) 3-D-seed models representing different stages of development: 12 DAF (a), 18 DAF (b), 21 DAF (c) and 30 DAF (d); endosperm (in red) is semi-transparent to allow view on embryo; bar: 1 mm. (E) Plot of the embryo, endosperm and seed coat volumes across different developmental stages (a–d), calculated from the 3-D-MRI data. (F) Virtual cross section of seed at stage b. (G) Plot of the calculated endosperm and embryo surface areas, based on the MRI data. Abbreviations: al – aleurone; ce – cellularized endosperm; ch – chalazal region; cot – cotyledon; ecv – endosperm central vacuole; em – embryo; en – endosperm; fn – funiculus; ps – pseudoseptum; ra – radicle; sc – seed coat; se – seed; va – valve.

resolution MRI approach is that the sugar content is not equally distributed, but rather compartmentalized within the endosperm. Our data point to effects of the endosperm on the microenvironment of embryo.

2.4. Quantitative profiling of endosperm composition and developmental changes

To comprehensively characterize the chemical composition of the endosperm and its developmental dynamics, we analyzed the concentrations of key soluble sugars, free amino acids, organic acids, inorganic anions and cations in the dissected endosperm fraction. We also measured a number of less abundant metabolic intermediates involved

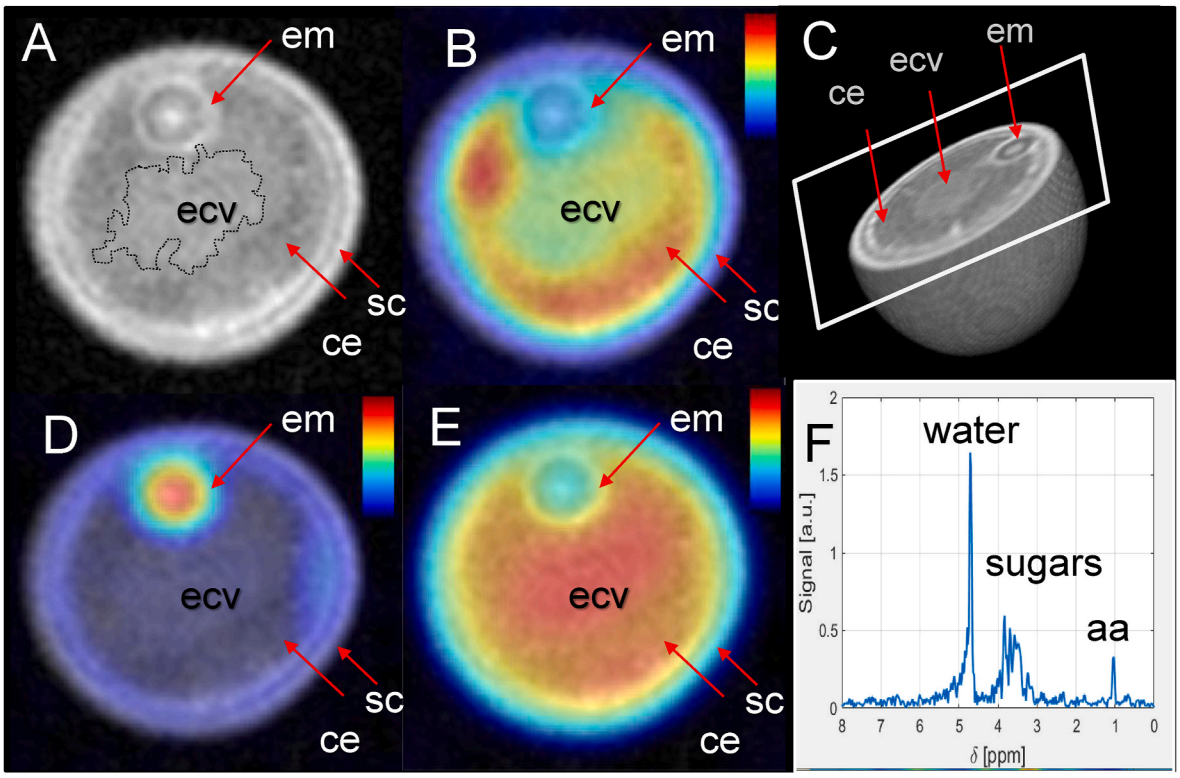

Fig. 3. Non-invasive mapping of metabolites in the embryo sac of a *B. napus* seed at 21 DAF. (A) Visualization of the embryo sac in the ^{1}H reference image showing *in vivo* the position of the seed coat, embryo and endosperm in the sampled tissue slice. The shape in the dotted line indicates an approximation of the central vacuole. (B) Visualization of sugar distribution within the seed. (C) Diagram indicating the virtual sectioning of the seed. (D) Visualization of lipid distribution. (E) Visualization of water distribution, obtained by integration of the chemical shift imaging spectra without VAPOR. (F) Spectral characteristics of the embryo sac content. The colored bars in (B, D and E) represent the color code for specific signal intensity. Abbreviations: aa – amino acids; ce – cellularized endosperm; ecv - endosperm central vacuole; em - embryo; sc - seed coat.

in energy metabolism (sugar breakdown, glycolysis, nucleotides and cofactors), with the majority also being quantified using external calibration schemes. In total, 77 compounds were assayed; an overview of the developmental profile of major groups is provided in Fig. 4A (full dataset in Supplemental Table 1). With the exception of the very early stages [9 days after flowering (DAF)], sugars were quantitatively the predominant endospermal compounds, with a switch from hexoses to sucrose occurring later in development. Notably, the proportion of glucose was significantly higher than that of fructose during most of the time analyzed (Fig. 4B). The second most abundant class of compounds was that of inorganic ions, predominated by potassium (~60%), followed by ammonium and chloride, while only trace amounts of nitrate were detected (Fig. 4C). The pool sizes of free amino acids and organic acids were similar (Fig. 4A). The free amino acid content was dominated by Gln, Glu, Ala, Val and Asp, contributing to 54–68% of the total amino acid pool in the endosperm throughout development (Fig. 4D). Among the organic acids, malate was the main constituent (~60%), followed by succinate (Fig. 4E). Energy metabolites made a very minor quantitative contribution, dominated by the glycolytic intermediate dihydroxyacetone phosphate (DHAP), followed by hexose phosphates and acetyl coenzyme A (Supplemental Fig. 1).

The total concentration of all quantified compounds together ranged from 170 to 360 mmol/l, reaching a maximum value at around 20 DAF; during this time the embryo exhibited expansion growth, accompanied by the onset of storage activity and accelerated uptake of assimilates. When the metabolite concentrations are taken as proxy for the osmolality of the endospermal liquid, we can conclude that sugars made the greatest contribution to the osmotic pressure of endosperm, except at very early development, during which our findings indicate a relatively high molar ratio of potassium versus sugars (Suppl. Fig. 2). This may have implications for regulation of expansion growth by potassium. The pH of the endosperm liquid fraction, measured using microsensors, was 5.9 ± 0.3 throughout development.

A time course of all measured metabolites/ions is represented as a heat map (Fig. 5), revealing certain general trends. The majority of amino acids increased in abundance over time (except for GABA and Asp, both in low abundance). Marked concentration shifts were observed for individual nucleotides with signaling functions (cyclic AMP), cofactors such as 5-methyl tetrahydrofolate (one-carbon metabolism), and inorganic ions (nitrate). Notably, trehalose-6-phosphate, regarded as a marker for sucrose availability, appears rather uncoupled from sucrose abundance based on the determined time courses.

2.5. Tracing sugar transport from silique to seed by isotope feeding

In vitro silique culture can be used to transfer (labeled) compounds toward the embryo. In the present study, we tested the validity of this approach to best mimic *in planta* conditions.

First, detached siliques were allowed to absorb a nutrient solution containing minerals, sugars and amino acids, and the embryo growth was assessed at several time points up to 8 days (Fig. 6A and B). This experiment revealed that embryos grown in silique culture accumulated biomass (dry weight) in a similar pattern as those grown *in planta*. No visible phenotype was observed for the embryos of the silique culture at any time point. Next, seeds at 15 and 30 DAF were incubated within the siliques to test the differences between developmental stages. The experiment revealed that the seeds at the earlier stage accumulated ~10% more ^{13}C-sucrose over time than those at the later stage (Fig. 6C). We further assessed whether seeds positioned along the silique reached a uniform biomass and received similar amounts of (^{13}C-labeled) sucrose

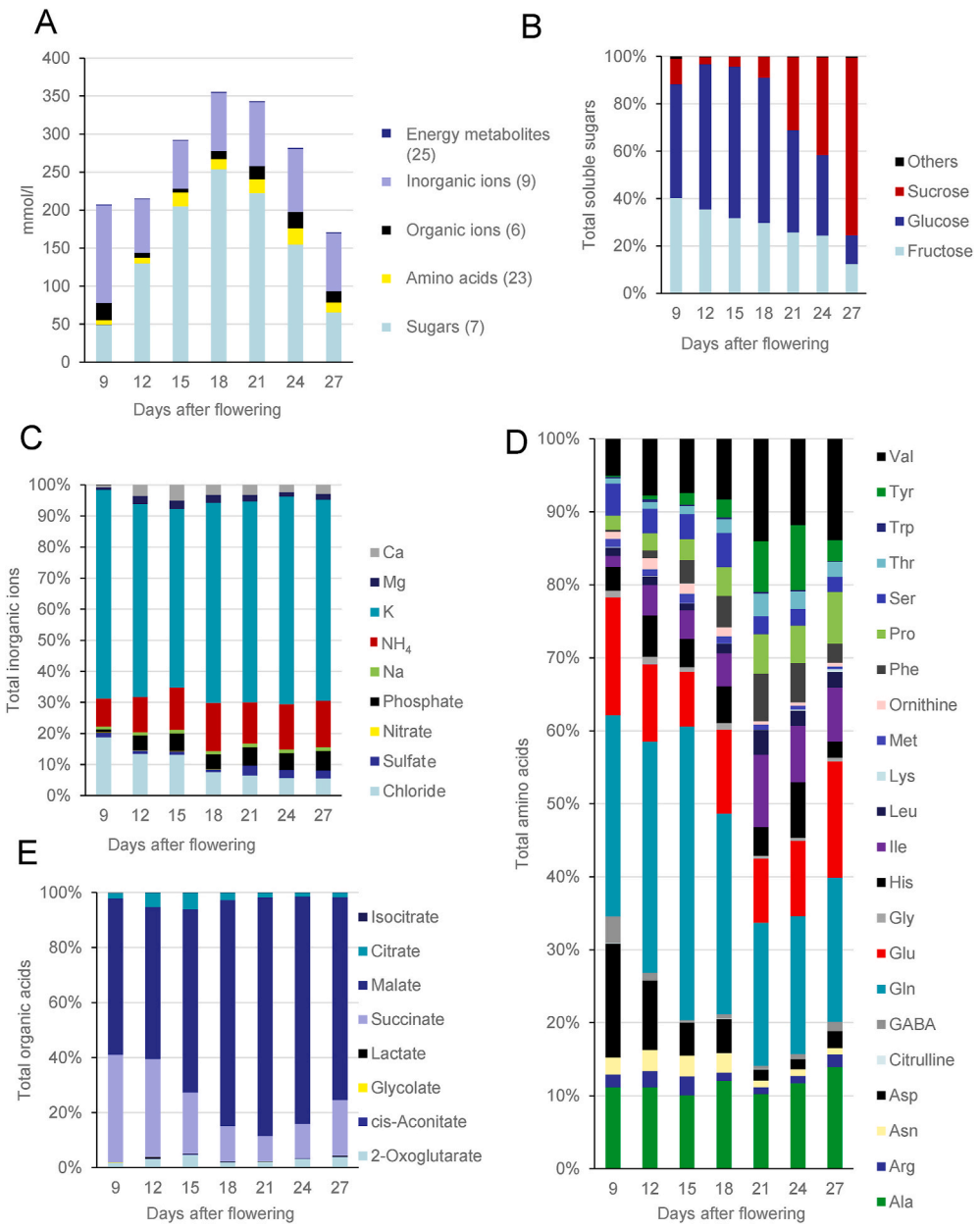

Fig. 4. Quantitative analysis of key organic and inorganic constituents of the endosperm in *B. napus* seeds. Plots of concentrations of (A) main categories of compounds at days 9–27 after flowering; (B) sugars; (C) inorganic ions; (D) free amino acids, (E) organic acids. Quantities were calculated based on averages from three biological replicates. See Suppl. Table 1 for details.

(Fig. 6D–F); our findings showed no positional effect on these two parameters. Finally, we measured the uptake rates of the seeds for ^{13}C-labeled glucose and sucrose, demonstrating that the accumulation of sucrose was constantly at least 7-fold higher than that of glucose (Fig. 6G). This finding is in agreement with the fact that sucrose is the natural (phloem-derived) carbon source for seeds *in vivo*, and was therefore used in further analysis of the dynamic of ^{13}C uptake into the seed.

2.6. *Temporal and satial dynamics of ^{13}C-sucrose transfer within the seed*

We investigated the kinetics and pool size of ^{13}C-sucrose accumulating in the various seed organs during the early cotyledon stage (~21 DAF) (Fig. 7A). To achieve this, isotope ratio MS was applied to dissected seed fractions (see Materials and Methods). At 4 h after the start of isotope provision, the ^{13}C label (absolute amount per organ) was observed to preferentially accumulate in the testa, while trace amounts were detected in the endosperm and embryo. At 8 h, the isotope abundance in the testa roughly doubled, the endosperm showed a significant accumulation of label, while in the embryo the label content remained very low. At 24 h, the label accumulation in the testa appeared to be approaching a plateau phase, while the accumulation in the endosperm continued a linear increase, indicating it to be the main storage pool of ^{13}C-labeled sucrose. The embryo also revealed a significant accumulation of label at this time point, but this remained lower than in the other organs. These data allow us to conclude that (i) the labeled ^{13}C-sucrose first arrives to the testa, and (ii) the endosperm serves as the main storage pool of sugars at the stage investigated here.

Using liquid chromatography-MS, we investigated the presence of sucrose variants in the endosperm, by means of distinct isotopic labeling (Fig. 7B). At 4 h after the start of isotope feeding, fully labeled ^{13}C-sucrose was detected, contributing to ~2% of the total sucrose pool. After

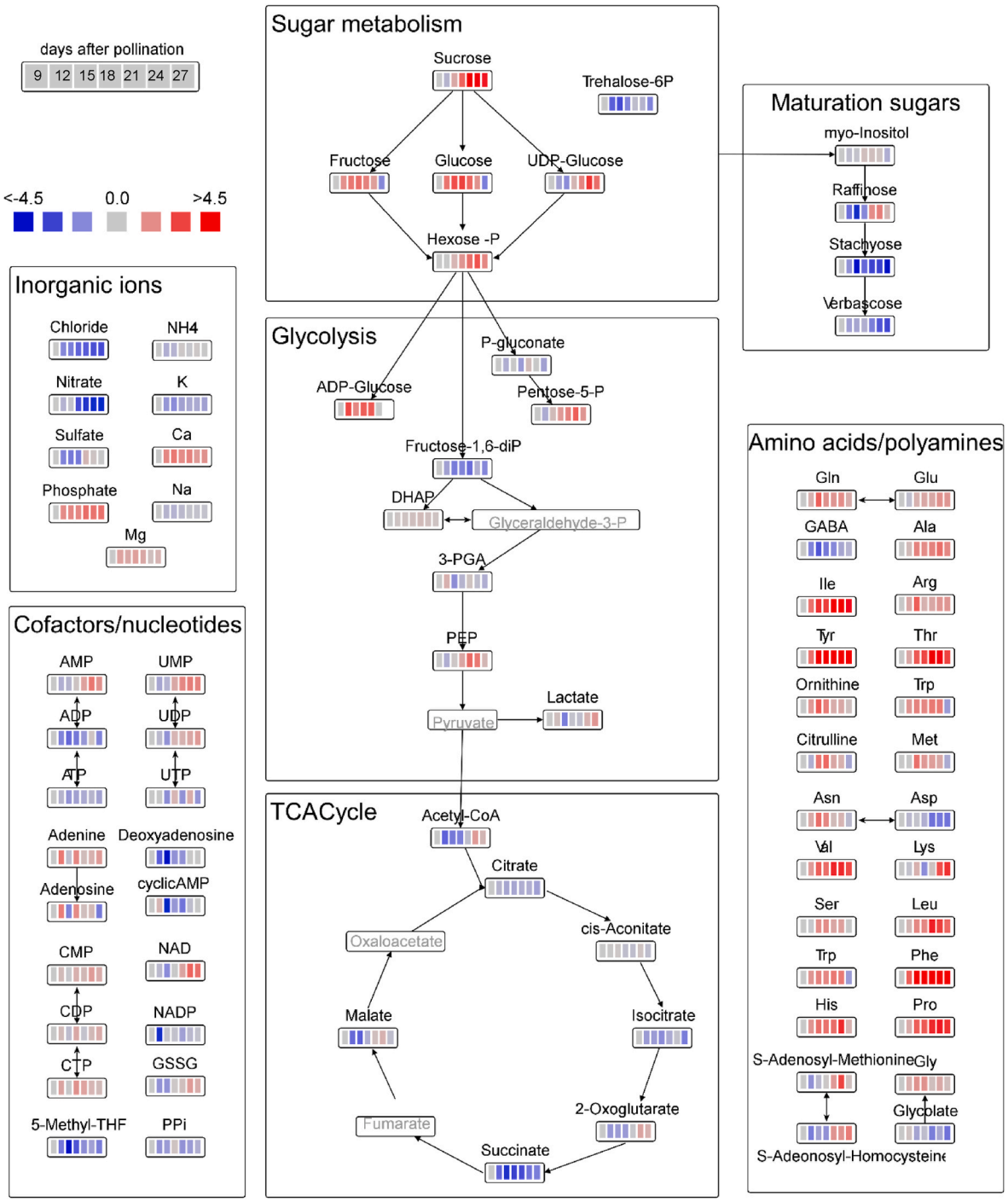

Fig. 5. Metabolic pathway map highlighting changes in the abundance of metabolites in the liquid endosperm fraction of *B. napus* seeds. Developmental changes between days 9 and 27 after flowering are given as heat map with fold-changes (log2 scale): decreased (blue) and increased (red) quantities relative to the value measured at day 9 after flowering. Values are averages from three biological replicates. Detailed metabolite data are provided in Suppl. Table 1 Abbreviations: 3-PGA - 3-phosphoglycerate; DHAP - dihydroxy acetone phosphate; GSSG - oxidized glutathione; PEP - phosphoenolpyruvate; THF - tetrahydrofolate.

8 h, its relative percentage approximately doubled and traces of other variants were also detected. After 24 h of silique culture, almost 20% of the total sucrose pool was labeled, the majority present as the fully labeled molecule (as used for feeding). This time course implies that the turnover time of sucrose in the endosperm under these conditions is ~5 days at the developmental stage of 21 DAF. During later development, the turnover times are expected to be much shorter, e.g. due to the decrease of the endosperm volume.

Matrix assisted laser/desorption ionization mass spectrometry imaging (MALDI-MSI) was used to spatially resolve sucrose transfer inside the seed at the heart stage of embryo development (corresponding microscopic image in Fig. 7C). Representative MS images at 2 h after feeding are shown in Fig. 7D–G. Analytes were predominantly detected as potassium adducts ($[M+K]^+$) due to the high potassium content of the seed (~60% of inorganic ions). The MALDI matrix signal was uniform across the seed section, ensuring uniform detection conditions (Fig. 7G). Unlabeled disaccharides, with the sum formula $C_{12}H_{22}O_{11}$, were detectable in all seed compartments, with slightly elevated signal intensities in the basal region of the testa (Fig. 7F). This signal corresponds to natural (unlabeled) sucrose. Disaccharides with the same mass, such

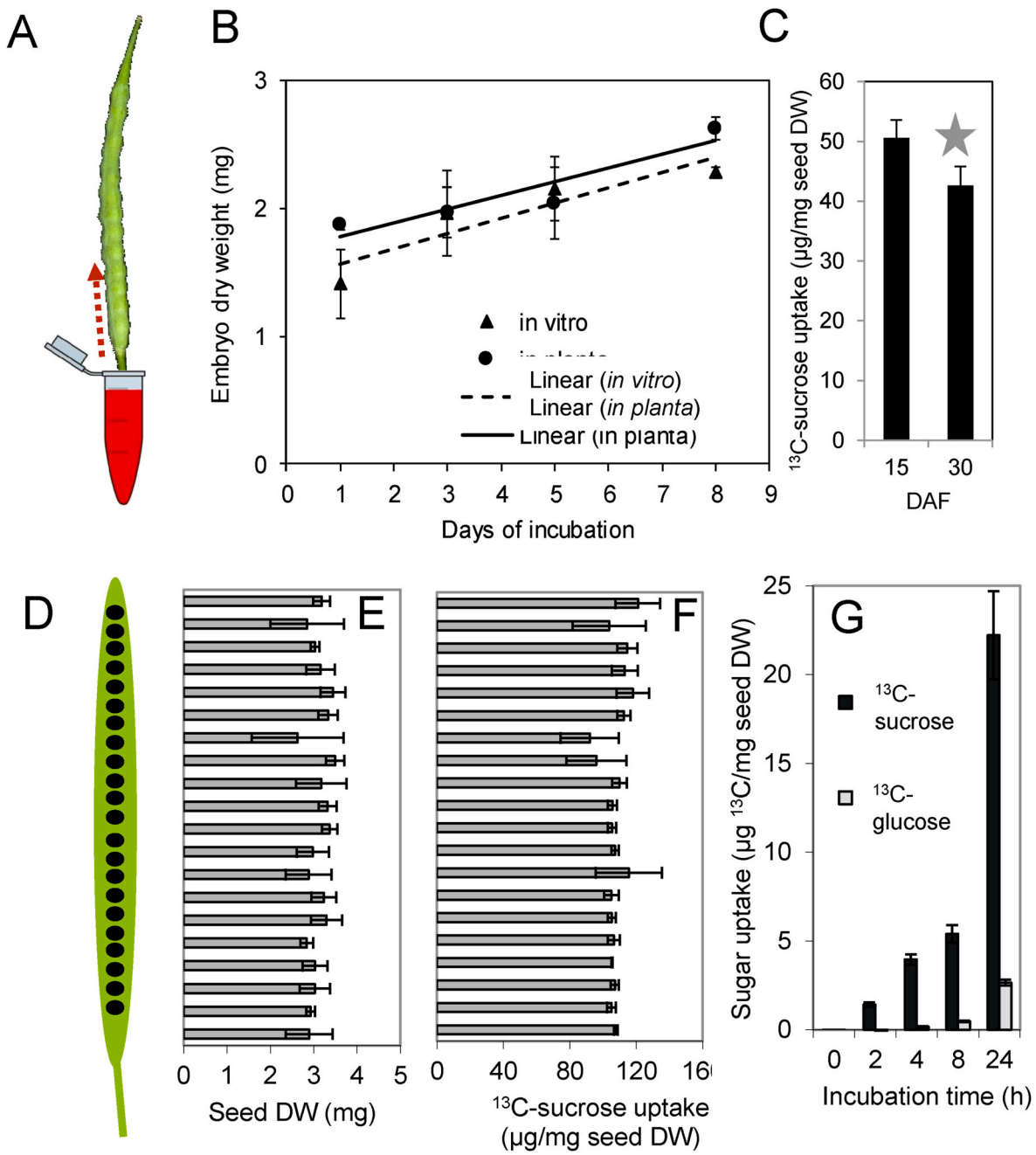

Fig. 6. Study of sugar uptake by developing seeds of *B. napus* in silique culture. (A) Experimental set-up for provision of substrate (feeding) during silique culture. (B) Changes in dry weight (DW) of embryos growing in silique culture (*in vitro*) versus those grown in siliques attached to the mother plant (*in planta*) over a time period of 8 days (incubation start at 25 DAF). (C) ^{13}C-sucrose uptake in seeds grown in silique culture for 24 h at 15 versus 30 DAF; the star indicates a statistically significant difference between the groups ($p<0.05$, *t*-test). (D) Diagram of a silique with individual seeds (25 DAF) sampled for (E) DW and (F) ^{13}C-sucrose uptake. (G) Comparison of ^{13}C-sucrose versus ^{13}C-glucose uptake in seeds grown in silique culture for up to 24 h. Values plotted in B-E are mean ± SD (n=5). Abbreviations: DAF - days after flowering; DW - dry weight.

as maltose or lactose, could have contributed, but these were not detected in our profiling (Fig. 4), and can therefore be ruled out. Most relevant to our interest was the pattern of fully labeled ^{13}C-sucrose, which was detectable in the branch point of the funiculus, starting to spread towards the interior, including the endosperm (Fig. 7E). Notably, the label accumulated in the epidermis layer and basal endosperm, but none was detected in either the suspensor or other parts of the embryo. At later time points, fully labeled sucrose was observed to spread throughout the seed, with the abundance being highest in the periphery (cellularized endosperm and seed coat) (data not shown).

An analysis of the early cotyledon stage revealed a similar pattern in label distribution at 2 h: the strongest signal of ^{13}C-sucrose was seen in the seed coat and basal cellularized endosperm, and a small amount of label was noted in the radicle tip (Supplemental Fig. 3). Unlabeled sucrose was detected throughout the seed, with the highest levels appearing in the basal seed coat/endosperm, and lowest levels in the endospermal central vacuole.

2.7. Studying nitrogen transfer to the seed

In vitro silique culture was also used to check the transfer of free amino acids. For this purpose, ^{15}N-labeled Gln was used, representing

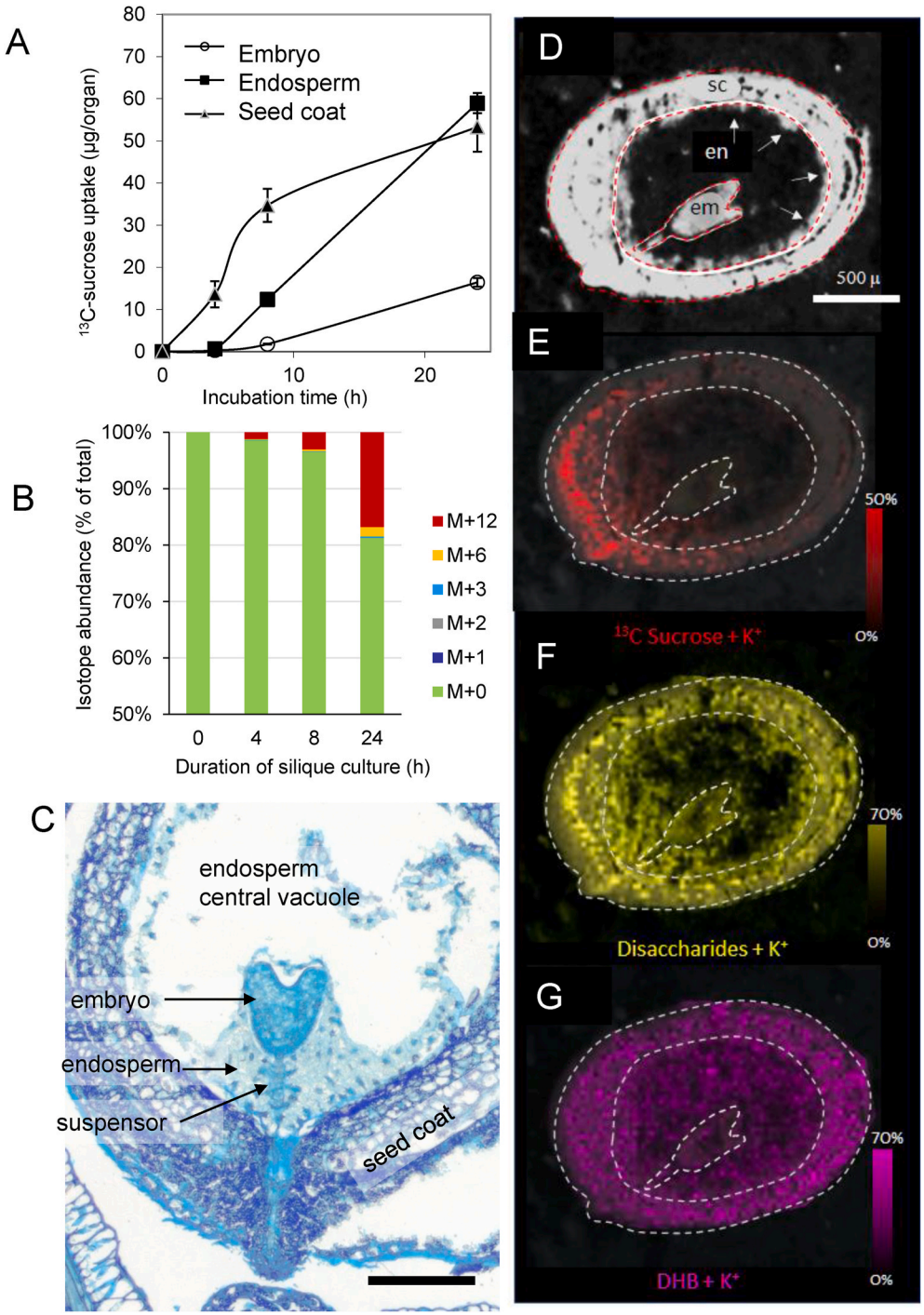

Fig. 7. Uptake and metabolism of ^{13}C-sucrose in the individual seed compartments in *B. napus*. (A) Comparison of ^{13}C-sucrose uptake in the embryo, endosperm and seed coat of seeds incubated in silique culture for up to 24 h; values plotted are mean ± SD (n=5). (B) Shift in isotope abundance for sucrose in the endosperm, measured using liquid chromatography–mass spectrometry over a 24-h time course of silique culture (note that y-axis starts at 50%); the digits indicate the number of ^{13}C atoms per molecule of sucrose (M corresponds to the unlabeled sucrose molecule while M+12 corresponds to full labelling). (C) Light microscope image of the embryo surrounded by the endosperm during the heart stage (toluidine staining). (D–G) Mass spectrometry images of seed sections (at 12 days after flowering) acquired using MALDI-FT-ICR-MS after feeding with ^{13}C-sucrose for 2 h. The images indicate (D) optical reference image of tissue section, (E) fully ^{13}C-labeled sucrose, (F) unlabeled disaccharides with the sum formula of $C_{12}H_{22}O_{11}$, and (G) DHB matrix. Abbreviations: DHB - 2,5-dihydroxybenzoic acid; em - embryo; en - endosperm; sc - seed coat.

the key phloem-derived amino acid in *B. napus* (Lohaus and Moellers, 2000), as well as the predominant amino acid present in its endosperm (Fig. 4). Upon feeding with ^{15}N-Gln for 24 h, label accumulation was measured in individual seeds using isotope ratio mass spectrometry, and Gln uptake rates were calculated (Supplemental Fig. 4A). Seeds positioned along the silique appeared to receive similar amounts of (^{15}N-labeled) Gln. As per ^{13}C-sucrose, the amount of label accumulated per seed organ was measured (Supplemental Fig. 4B). The measured net ^{15}N-Gln uptake rates over 24 h were found to be highest for the testa, followed by the endosperm, and lowest for the embryo. Therefore, the testa appeared to be the largest Gln sink (at least during the relatively short time course studied). To test whether some of the delivered Gln was also actively metabolized, we assessed the presence of the ^{15}N-label in other amino acids (Supplemental Fig. 4C). When calculating the label proportions, we determined that ~35% of the total Gln pool in the testa was labeled after 24 h. The label also appeared in significant amounts in Glu and Ala, and in smaller fractions in the other sampled amino acids (Pro, Val, Leu, Thr and Ser). This label transfer is indicative of underlying metabolic reactions and networks.

Finally, we tested the kinetics of ^{15}N-ammonium uptake in the seeds and the response to illumination (Supplemental Fig. 4D). Isotope ratio MS was applied to whole seeds collected after 2, 4, 6 and 8 h of feeding. The findings revealed a substantial effect of light on the isotope uptake rate into the seeds (approximately double the uptake rate under light conditions versus dark), highlighting the relevance of environmental conditions for assimilate uptake.

3. Discussion

3.1. Mechanistic view of the endosperm role in Brassicaceae early seed development

Our study provides *in vivo* evidences for the metabolic dominance of endosperm over the embryo during pre-storage phase of development in oilseed rapeseed. This phenomenon is likely predetermined by the origin of endosperm: "with an excess of maternal chromosomes over paternal ones, the mother can exert greater control over nutrient allocation to the progeny in relation to her own fitness" (Baroux et al., 2002). The diploid embryo and the triploid endosperm are enclosed completely by the testa, thus sharing space and nutrients (Figs. 1 and 2). Nutrient uptake by the embryo and endosperm therefore occurs via the surface areas facing the apoplast. While the embryo grows as a multicellular structure (small, densely packed cells), the endosperm initially avoids formation of cell walls and instead forms a giant multinuclear cytoplasm (coenocyte). During development, the endospermal coenocyte surface rapidly enlarges due to the formation of a thin layer of cytoplasm underlying the testa, and at the same time envelops the embryo. In the proximity of the embryo (micropylar chamber) the endosperm is cellularized throughout (Fig. 7C), whereas its chalazal part is the last to cellularize (Van Lammeren et al., 1996). The endosperm acquires unlimited access to any nutrients released from the testa and is in a prioritized position for assimilate uptake/utilization. This implies metabolic dominance of the endosperm over the embryo, which can be interpreted as a growth constraint for the embryo (Ungru et al., 2008). The endosperm (along with the testa) defines the sink strength and accumulates osmolytes driving water uptake, cell expansion and gain in seed size. Endosperm development culminates in complete cellularization and differentiation of endosperm epidermis into aleurone. At this stage, the seed already reaches ~61% of its final volume, while the embryo contributes to just 1% of this (Fig. 2). The embryo appears to bear no impact on seed size – seed coat development/seed size has been shown to be unaffected in seeds of embryo-free *Arabidopsis* mutants (Xiong et al., 2021).

A consequence of the embryo-endosperm inequality is that the endosperm is the main carbon sink for nutrients during the early stages of seed development (Figs. 3B and 7A). However, the biosynthetic capabilities of the endosperm are rather poor, and deposition of starch, oils and storage proteins occurs only in the aleurone layer (Borisjuk et al., 2013a,b). The endosperm preferentially accumulates soluble compounds. As its storage capacity is limited, unutilized sugars migrate toward the interior (facilitated by the activity of SWEET transporters; Chen et al., 2015), eventually becoming available to the embryo. To our understanding, such outsourcing can be described as overflow metabolism rather than a kind of 'altruistic behavior', as has frequently been used to describe the relationship between the endosperm and embryo. The embryo has the opportunity to boost its growth only after the endosperm satisfies its own demand for growth and storage, and accomplishes its own developmental program by transition to programmed cell death (see also Ingram, 2017).

The embryo becomes the main sink within the seed, accumulates biomass and increasingly occupies the seed interior volume by replacing the endosperm. This embryonic boost requires an increase in nutrient uptake from the surrounding endosperm, which is accomplished in two ways: first, the rise in sugar levels in endosperm/apoplast (sugars are known inducers of transfer cell differentiation) (Patrick and Offler, 2020); secondly, the embryo surface enlarges during morphological transitions from the globular to torpedo and cotyledon stages. MRI modeling revealed that, with the formation of cotyledons, the embryo surface area increases substantially (Fig. 2). Cellularization of the endosperm, already observed at the heart stage of the embryo (Fig. 7C), precedes (but does not cause) the embryonic switch to maturation, in agreement with recent findings on *Arabidopsis* (O'Neil et al., 2019). It is rather the developmental death of the endosperm (Xiong et al., 2021), in part mediated by mechanical stress (Fourquin et al., 2016), which allows the embryo to win the competition for assimilates and space.

Despite this switch in dominance, the endosperm keeps some control over the embryo's environment. During development, the lipid-enriched aleurone forms an isolation barrier which completely encloses the seed interior except its chalazal region (Fig. 1C and Supplemental Movie 2). The chalazal seed coat of *B. napus* serves as the first point of entry, which is anatomically and transcriptionally specialized for nutrient transport (Ziegler et al., 2019). It is the portal for nutrients in *Arabidopsis* (Stadler et al., 2005; Werner et al., 2011; Geist et al., 2019). Specialization of the endosperm within this region appears to be a common feature not only in *B. napus* and *Arabidopsis*. The lack of lipid accumulation and formation of endosperm transfer cells at the nutrient delivery gate (nucellar projection) is documented also in grasses like *Hordeum* sp. and *Triticum* sp. (Brown et al., 1999; Melkus et al., 2011; Rolletschek et al., 2015; Radchuk et al., 2019; Olsen, 2020). Due to the persistence of aleurone in the mature seed, the endosperm keeps control over the metabolic environment of the embryo even after maturation, affecting seed dormancy (Penfield, 2017) and germination (Munz et al., 2017). The picture of the endosperm's role in evolution of the flowering plant is still evolving.

3.2. Osmotic species in the B. napus endosperm and implications for early seed expansion growth

Sugars account for 50–70% of phloem sap osmolality (Patrick and Offler, 2001), and, as evidenced in the present study, this also applies to the endosperm sap of *B. napus* (Fig. 3A). In the phloem, sucrose is normally of particular relevance; however, the *B. napus* endosperm predominantly accumulates hexoses (at early-to mid-stage, due to high local invertase activity; see also Hill et al., 2003). Therefore, invertases play an important role in maintaining high osmotic pressure inside the endosperm as the seed is expanding. Potassium is another major osmotic species in phloem sap (Patrick and Offler, 2001), where it can interchange with sucrose to sustain sap osmolality.

Notably, the present data imply that potassium serves an unprecedented role in the endosperm, with a two-fold significance: (1) in the early stage, potassium is the main osmotically active constituent in the endosperm fluid (Fig. 4A and C), making it the main driver of turgor, needed for expansion growth. A valid hypothesis is that potassium accumulation in the endosperm drives water uptake during very early stages of seed development, leading to expansion and seed growth. (2) Another likely function for potassium is the so-called 'potassium battery' (Gajdanowicz et al., 2011). For phloem, it is known that potassium efficiently stimulates the plasma membrane H^+-ATPase, energizing transmembrane transport processes and, eventually, sugar loading into the phloem sap. Potassium serves as a decentralized energy storage, and could act as such in the seed by overcoming local energy limitations. Genetic studies have demonstrated the importance of potassium and its transporters for normal seed development. Functional cation/H^+ exchangers (CHX17 and CHX18) promote early embryo development through the endosperm where these genes are expressed (Padmanaban et al., 2017). Knockout of intracellular Na^+/H^+ (NHX) antiporters (mediating vacuolar K^+/H^+ exchange) compromises cell elongation, and generate siliques with few or no seeds (Bassil et al., 2011). It should also be noted that potassium is not just a vacuolar osmoticum, driving turgor and cellular expansion, but also exists in significant amounts in the cytosol, where it is critical for protein function/stability and as an enzyme cofactor. In-depth studies on the dynamics of potassium in the endosperm are required to elucidate its relevance for normal seed development. It is possible that manipulation of potassium transporters offers novel avenues to stimulate seed growth/size, representing a major breeding and biotechnology target.

3.3. Homeostasis versus imbalance (change) in endosperm composition

A proposed metabolic function of the endosperm is that the young

embryo develops within a homeostatic environment, somehow uncoupled from external constraints (Melkus et al., 2009). For example, any immediate physiological and/or environmental effect on phloem transport will be buffered by the large sugar pool stored in the endosperm. This may be necessary to sustain embryogenesis, although our findings also indicate that the metabolic equilibrium is not fixed, but underlies a developmental dynamic (Figs. 4 and 5). A prominent example is the well-known hexose/sucrose switch during mid development, previously described in *B. napus* (Hill et al., 2003) and other species (Weber et al., 2005).

The pool of carbon and nitrogen stored in the endosperm is not just that remaining from the phloem (i.e. not used up), but rather it results from active metabolism and selective demand by both the embryo and endosperm. For example, the imbalance found herein between glucose and fructose in the endosperm (Fig. 4B) hints to selective demands. Indeed, Hill et al. (2003) pointed out that the *B. napus* embryo likely favors fructose rather than glucose, evidenced by almost double the uptake rate for fructose (versus glucose) and double the enzyme activity of fructokinase (versus glucokinase). Another example is the amino acid composition of the endosperm (Fig. 4D), which differs significantly from that of the phloem (Lohaus and Moellers, 2000). In the latter, the predominant amino acids are Gln and Glu, followed by Ser, Asp and Thr. This difference indicates active amino acid metabolism in the endosperm (and testa) of *B. napus,* in agreement with the findings that endosperm cells express the enzymatic machinery needed for active amino acid synthesis (Lorenz et al., 2014), and substantial amounts of storage protein are accumulated in the aleurone layer (Borisjuk et al., 2013a,b). Several complex biological mechanisms govern the metabolic activity of the endosperm, and that biochemical analyses can provide important links to the tripartite metabolic interactions between the testa, endosperm and embryo.

3.4. Imaging technologies for understanding assimilate allocation in seeds

We examined *B. napus* seeds and characterized the metabolic environment of the embryo using various state-of-the-art approaches. However, none of these approaches alone was sufficiently informative to achieve our goal. The embryo is buried deep inside the seed, making the analysis difficult. Observation by means of a light microscope can allow detection of endosperm cellularization and embryo structures only after dissection of the seed. Reconstruction of volumetric relationships is difficult (Ohto et al., 2009), as is biochemical analysis of the tissues. Fast-freezing of the seed, followed by cryosectioning, enables the observation of snap shots of the tissues and, thereby, precise reflections of the metabolic conditions (Schiebold et al., 2011). MSI is appropriate for this purpose, by providing high chemical resolution (Boughton et al., 2016). MSI was therefore the method of choice for tracing ^{13}C-labeled sucrose in order to uncover the pathway of sugar allocation within the seed. Infrared-based microspectroscopy also enables the visualization of sucrose in seeds at a microscopic level of resolution (~12 μm) (Guendel et al., 2018). It should also be considered that reconstruction of 3-D metabolite distributions based on destructive sampling is challenging due to significant time requirements for data acquisition and processing, though not impossible (Sturtevant et al., 2017; Boughton et al., 2019).

In vivo assays are the desired approaches for the study of seeds. X-ray tomography provides extremely high spatial resolution for 3-D-modeling and structural studies (Verboeven et al., 2013). Its drawback, however, is that it cannot provide chemical resolution and relies on ionizing radiation, which excludes long time monitoring of development. In the present study, we applied MRI, which is limited in spatial resolution, but is capable of non-invasive structural and chemical imaging of a living object. *In vivo* MRI is particularly relevant for the cases of soft or fluid tissues, such as the central endosperm vacuole in rapeseed. Tissue quality is not compromised by preparation (no freezing, sectioning, embedding), and volumetric assays based on MRI, as used herein, reflect the real spatial relationships inside of the living seed. We show here how MRI integrates structural and metabolic features of the seed interior. The endosperm dominates in size and largely influences the microenvironment of embryo during early development. Combining of *in vivo* observations (MRI) with other approaches can help to understand how a gradient of sugars and other factors inside of developing seeds (including hormones and physical interactions; see Wang et al., 2019; Rolletschek et al., 2020; Ingram et al., 2020; Lu et al., 2021) could act as a positional signal for cells and orchestrate embryogenesis.

Overcoming of barriers in resolution and sensitivity in the field of *in vivo* imaging (Sturtevant et al., 2020; Van Schadewijk et al., 2020) provides unique opportunities to examine different cell types even in small seeds. It is expected that the detection of metabolite gradients across tissues and apoplastic interfaces will fill certain gaps in our understanding of fundamental processes in seed biology. Overall, spatially resolved metabolite analysis and imaging can provide valuable information to ongoing research.

4. Materials and methods

4.1. Plant material, growth conditions and sampling

Plants of *B. napus* (cultivar Westar) were grown in a glasshouse under conditions of 22±2 °C, a 16-h photoperiod (250 mmol quanta $m^{-2}s^{-1}$), and 60% relative humidity. Plant growth was restricted to the main stem and two lateral stems; side shoots were removed upon emergence. Flowers were tagged on the day of anthesis. At the desired stage, seeds were quickly isolated from intact siliques and opened with a scalpel under a dissecting microscope. Distinct volumes of the liquid endosperm fraction were collected using a Hamilton microliter syringe (600 series) and snap-frozen. In certain cases, the remaining testa and embryo were also sampled. Prior to snap-freezing, the testa/embryo tissue was dipped twice into distilled water and softly blotted with tissue paper in order to remove any endospermal liquid from its surface. Three to five biological replicates per time point were collected, with each sample consisting of at least three individual seeds.

4.2. Microsensor-based pH analysis of the liquid endosperm fraction

All pH data were recorded using the microsensor pH-1 micro (PreSens GmbH, Regensburg, Germany). Fresh seeds were cut to allow immediate entry of the microsensor into the seed interior. The sensor tip (~50 μm) was immersed in the endosperm liquid for at least 4 min to allow full equilibration. Sensor calibration was performed using calibration standards (pH 5, 6, 7, 8, 9), according to the manufacturer's instructions.

4.3. Silique culture and isotope labeling procedures

For isotope labeling in seeds within intact siliques, the siliques were detached from the plant with a scalpel and immediately placed in a solution containing 25% Murashige and Skoog medium and 2 mM MES at a pH of 5.6 (all Sigma-Aldrich Chemie GmbH, Taufkirchen, Germany). For the experiments on tracing sugar uptake, the medium also contained 100 mM [UL-$^{13}C_{12}$]-sucrose or [UL$^{13}C_6$]-glucose (Campro Scientific GmbH; Berlin, Germany) and 50 mM unlabeled Gln. For the experiments on tracing amino acid uptake, the medium contained 100 mM unlabeled sucrose and 50 mM [$^{15}N_2$]-Gln (Campro Scientific GmbH). In some cases, labeled Gln was replaced with 50 mM ^{15}N-labeled NH_4Cl. The incubation time varied for the different experiments as described in each section. Please note that siliques were gently surface-sterilized, and all liquids/materials/incubations flasks were made sterile before use. Incubation was performed in a glasshouse to ensure stable growth conditions. Following incubation, the seeds were removed from the siliques and either frozen intact or rapidly dissected into the embryo, endosperm and testa fractions. The material was snap-frozen in liquid nitrogen and stored at −80 °C until further use.

4.4. Biochemical analysis using liquid chromatography and mass spectrometry

For targeted analyses, frozen material (testa/embryo) was homogenized in 1.5-mL microcentrifuge tubes (Eppendorf AG, Hamburg, Germany) by manual grinding with a pestle. The samples were then extracted with 1:1 (v/v) methanol/chloroform containing 2.5 nmol acephate (Sigma-Aldrich Chemie GmbH) as an internal standard in a Retsch TissueLyser (Qiagen GmbH, Hilden, Germany) for 180 s at 1800 strokes per second (racks precooled to −80 °C). Subsequently, distilled water was added to achieve two layers, and the samples were centrifuged at 2000 g for 5 min. The main fragment of the upper water/methanol layer was filtered through Vivaclear centrifugal filters (0.8 µm pore size; Sartorius Stedim Biotech GmbH, Göttingen, Germany) at 2000 g for 2 min. The endosperm was diluted 10-fold with 1:1 water/methanol (incl. internal standard) and filtered by same Vivaclear centrifugal filters.

The analyses of soluble sugars, organic acids, amino acids and other organic intermediates were performed by means of hydrophilic interaction chromatography coupled to triple-quadrupole MS, as described previously (Schwender et al., 2015). Absolute quantification of metabolites was performed, following external calibration with authenticated standards. All $^{13}C/^{15}N$-labeled intermediates were measured using the same method, but applying distinct MS detection parameters, as listed in Supplemental Table 2.

Analysis of inorganic ions was performed using ion chromatography (ICS-3000 system, Dionex GmbH, Idstein, Germany) with suppressed conductivity detection. For anions, the IonPac AS19 (250 × 2 mm^2) analytical column and its respective guard column (AG19) were used in an isocratic run with 20 mM NaOH as the mobile phase. For cations, the IonPac CS16 (250 × 5 mm^2) analytical column and its respective guard column (CG16) were used in an isocratic run with 26 mM methanesulfonic acid as the mobile phase. All solutions were prepared according to the manufacturer's instructions, using ultrapure water with a specific resistance of 18.2 MΩ cm (Millipore; Merck KGaA, Molsheim, France). Commercially available certified standard solutions (Dionex™ Combined Standards; Thermo Fisher Scientific, Inc., Sunnyvale, CA, USA) were used for external calibration.

4.5. MRI, MR spectroscopy and modeling

MRI and MRS experiments were performed using a Bruker Avance III™ HD 400 MHz NMR spectrometer (Bruker BioSpin GmbH, Rheinstetten, Germany) equipped with a 1000 mT/m gradient system and resonators with inner diameter of either 10 mm or 25 mm. For displaying the 3-D morphology and volumetric analysis of living seeds an adjusted spin echo sequence to measure water and lipid simultaneously was used (Munz et al., 2017). Global frequency-selective RF pulses ("calculated" shape with bandwidth 1500 Hz) facilitated the separate excitation of water or lipid. An interleaved acquisition scheme was conducted as described earlier (Munz et al., 2016). For modeling of living seeds inside of a silique, a water and lipid image with isotropic resolution of 70 µm was acquired by using a repetition time (TR) of 400 ms; echo time (TE), 6 ms; number of averages (NA) 4; field of view (FOV) 11 x 7.5 × 7.5 mm^3; matrix size 157 x 107 x 107. Additionally, a similar measurement of another silique was conducted with the same sequence parameters but a larger FOV (30 x 14.5 × 14.5 mm^3, matrix size 375 x 181 x 181) and NA=1. For 3-D-models of single seeds, MR images with an isotropic resolution of 70 µm were utilized; the sequence parameter were as follows: TR, 400 ms; TE, 6.1 ms; NA, 4; FOV 12 x 6 × 6 mm^3; matrix size 100 x 93 x 93.

For the MR spectroscopy measurements on a rapeseed, a proton reference image of the examined slice (thickness 350 µm) was acquired using a rapid acquisition with relaxation enhancement (RARE) sequence with TR, 1000 ms; TE, 5 ms; resolution, 50 × 50 µm2; NA, 16; RARE factor 4. The local distribution of sugars and lipids was detected with a slice-selective chemical shift imaging (CSI) method applied in spin-echo mode (total measurement time, 41 min 32 s). The sequence parameters were as follows: TR, 1000 ms; TE, 1.2 ms; field of view, 2.8 × 2.8 mm^2; resolution, 165 × 165 μm^2; number of scans, 2492. The experiment was performed with and without water suppression (VAPOR; pulse bandwidth, 250 Hz). The metabolite images were calculated by integrating the corresponding peak areas.

Image reconstruction was performed using MATLAB (MathWorks; https://mathworks.com/).

Segmentation and seed modeling were performed using AMIRA 2020.3 (Thermo Fisher Scientific, Inc.), as described previously (Borisjuk et al., 2013a,b).

4.6. MALDI-MSI procedures

Incubated seeds were typically flash frozen in liquid nitrogen and stored at −80 °C to prevent enzymatic degradation or analyte migration. Subsequently, samples were cryosectioned to a thickness of 30–50 µm. Carboxymethyl cellulose was used as an MSI-compatible embedding medium. Tissue sections were thaw-mounted and dried in a desiccator at reduced pressure (Boughton and Thinagaran, 2018). Matrix, 2,5-dihydroxybenzoic acid (50 mg/mL in acetone) was applied with a TM-Sprayer (HTX Imaging, Chapel Hill, NC, USA) (1200 mm/min nozle transit speed, a flow rate of 150 µL/min, drying gas temperature set to 30 °C, using 1.5 mm track spacing with 0.75 mm track offset for repeat passes, a total of 4 passes were conducting using an alternating criss-cross pattern) coupled to a Shimadzu LC-20AD pump (Shimadzu Corporation, Kyoto, Japan). MALDI-FT-ICR-MS (Solarix 7T XR; Bruker Corporation, Billerica, MA USA) was used in the positive ion mode with optimized ion transfer settings across the mass range 200–1500 *m/z* using a data size of 2M providing a mass resolution of >120,000 at 400 *m/z*. The MS was calibrated with elemental red phosphorous clusters. For imaging tissue sections, the laser was set to 37% power, using the minimum laser spot size, 2000 shots were fired at 2 kHz for each pixel to specifically detect unlabeled and ^{13}C-labeled compounds with a raster of 25 × 25 µm. Sucrose was observed as $[M+K]^+$ *m/z* 381.07953 (theoretical $C_{12}H_{22}O_{11}K^+$ *m/z* 381.079369, 0.42 ppm mass error), ^{13}C-sucrose as $[M+K]^+$ *m/z* 393.11959 (theoretical $^{13}C_{12}H_{22}O_{11}K^+$ *m/z* 393.119627, 0.09 ppm mass error).

4.7. Isotope ratio MS and calculation of uptake rates

To analyze the incorporation of ^{13}C- or ^{15}N-label into the plant material, freeze-dried pulverized samples were used for elemental analysis coupled to isotope ratio MS (EA-IRMS; Elementar Analysensysteme GmbH, Langenselbold, Germany) according to the manufacturer's protocols, and acetanilide was used as a calibration standard. From the $^{12}C/^{13}C$ (or $^{14}N/^{15}N$) ratio, the uptake rates were calculated taking into account the total amount of carbon (or nitrogen), the material dry weight and the incubation time. Potential respiratory loss of ^{13}C-label during incubation was not taken into account, possibly leading to slight underestimation of the actual carbon uptake rates.

4.8. Histology

All histological procedures performed in the present study are described in detail elsewhere (Borisjuk et al., 2013a,b).

Declaration of competing interest

The authors declare that they have no known competing financial interests or personal relationships that could have appeared to influence the work reported in this paper.

Acknowledgements

We thank L. Kalms for support in seed modeling, Dr. E. Munz and Dr. T. Neuberger for MRI and Dr. N. Heinzel for support in mass spectrometry. LB and HR further acknowledge funding by the BMBF (AVATARS-project, grant no. 031B0770A), European Regional Development Fund (ERDF) and the Deutsche Forschungsgemeinschaft (grant no. 397750294).

Appendix A. Supplementary data

Supplementary data to this article can be found online at https://doi.org/10.1016/j.jplph.2021.153505.

Author contributions

L.B. and H.R. designed and carried out the research, analyzed data, and wrote the article.

S.M., S.W., S.O. and L.B. were responsible for MRI. B.B. and U.R. were responsible for MSI. H.R. and C.K. were responsible for biochemical analysis.

References

Baroux, C., Spillane, C., Grossniklaus, U., 2002. Evolutionary origins of the endosperm in flowering plants. Genome Biol. 3 reviews1026.1.

Bassil, E., Tajima, H., Liang, Y.-C., Ohto, M., Ushijima, K., Nakano, R., Esumi, T., Coku, A., Belmonte, M., Blumwald, E., 2011. The *Arabidopsis* Na^+/H^+ antiporters NHX1 and NHX2 control vacuolar pH and K^+ homeostasis to regulate growth, flower development, and reproduction. Plant Cell 23, 3482–3497.

Baud, S., Kelemen, Z., Thevenin, J., Boulard, C., Blanchet, S., To, A., Payre, M., Berger, N., Effroy-Cuzzi, D., Franco-Zorrilla, J.M., et al., 2016. Deciphering the molecular mechanisms underpinning the transcriptional control of gene expression by L-AFL proteins in *Arabidopsis* seed. Plant Physiol. 171, 1099–1112.

Baud, S., Wuillème, S., Lemoine, R., Kronenberger, J., Caboche, M., Lepiniec, L., Rochat, C., 2005. The AtSUC5 sucrose transporter specifically expressed in the endosperm is involved in early seed development in *Arabidopsis*. Plant J. 43, 824–836.

Bernstein, M.A., King, K.F., Zhou, X.J., 2004. Handbook of MRI Pulse Sequences. Elsevier/Wiley.

Borisjuk, L., Neuberger, T., Schwender, J., Heinzel, N., Sunderhaus, S., Fuchs, J., Hay, J. O., Tschiersch, H., Braun, H.P., Denolf, P., Lambert, B., Jakob, P.M., Rolletschek, H., 2013a. Seed architecture shapes embryo metabolism in oilseed rape. Plant Cell 25, 1625–1640.

Borisjuk, L., Rolletschek, H., Neuberger, T., 2012. Surveying the plant's world by magnetic resonance imaging. Plant J. 70, 129–146.

Borisjuk, L., Rolletschek, H., Neuberger, T., 2013b. Nuclear magnetic resonance imaging of lipid in living plants. Prog. Lipid Res. 52, 465–487.

Boughton, B.A., Thinagaran, D., 2018. Mass spectrometry imaging (MSI) for plant metabolomics. In: António, C. (Ed.), Plant Metabolomics. Methods in Mol. Biol., vol. 1778, pp. 241–252.

Boughton, B.A., Thinagaran, D., Sarabia, D., Bacic, A., Roessner, U., 2016. Mass spectrometry imaging for plant biology: a review. Phytochemistry Rev. 15, 445–488.

Boughton, B.A., Thomas, O.R.B., Demarais, N.J., Trede, D., Swearer, S.E., Grey, A.C., 2019. Detection of small molecule concentration gradients in ocular tissues and humours. J. Mass Spectrom. 55 (4), e4460.

Brown, R.C., Lemmon, B.E., Nguyen, H., Olsen, O.A., 1999. Development of endosperm in *Arabidopsis thaliana*. Sex Plant Reprod 12, 32–42.

Chalhoub, B., Denoeud, F., Liu, S., Parkin, I.A., Tang, H., et al., 2014. Early allopolyploid evolution in the post-neolithic *Brassica napus* oilseed genome. Science 345, 950–953.

Chan, A., Belmont, M.F., 2013. Histological and ultrastructural changes in canola (Brassica napus) funicular anatomy during the seed lifecycle. Botany 91 (10), 671–679.

Chen, L.-C., Lin, I.W., Qu, X.-Q., Sosso, D., McFarlane, H.E., Londoño, A., Samuels, A.L., Frommer, W.B., 2015. A cascade of sequentially expressed sucrose transporters in the seed coat and endosperm provides nutrition for the *Arabidopsis* embryo. Plant Cell 27, 607–619.

Clarke, W.E., Higgins, E.E., Plieske, J., Wieseke, R., Sidebottom, C., et al., 2016. A high-density SNP genotyping array for Brassica napus and its ancestral diploid species based on optimised selection of single-locus markers in the allotetraploid genome. Theor. Appl. Genet. 129, 1887–1899.

De Giorgi, J., Piskurewicz, U., Loubery, S., Utz-Pugin, A., Bailly, C., Mène-Saffrané, L., et al., 2015. An endosperm-associated cuticle Is required for *Arabidopsis* seed viability, dormancy and early control of germination. PLoS Genet. 11 (12), e1005708.

Fernie, A.R., Bachem, C.W.B., Helariutta, Y., Neuhaus, H.E., Prat, S., Ruan, Y.-L., Stitt, M., Sweetlove, L.J., Tegeder, M., Wahl, V., Sonnewald, S., Sonnewald, U., 2020. Synchronization of developmental, molecular and metabolic aspects of source–sink interactions. Nat. Plants 6, 55–66.

Figueiredo, D.D., Köhler, C., 2018. Auxin: a molecular trigger of seed development. Genes Dev. 32 (7–8), 479–490.

Fourquin, C., Beauzamy, L., Chamot, S., Creff, A., Goodrich, J., Boudaoud, A., Ingram, G., 2016. Mechanical stress mediated by both endosperm softening and embryo growth underlies endosperm elimination in *Arabidopsis* seeds. Development 143, 3300–3305.

Fuchs, J., Melkus, G., Borisjuk, L., Jakob, P., 2015. Tracking metabolite dynamics in plants via indirect ^{13}C chemical shift imaging with an interleaved variable density acquisition weighted sampling pattern. Magn. Reson. Mat. Phys. 28, 127–134.

Gajdanowicz, P., Michard, E., Sandmann, M., Rocha, M., Corrêa, L.G.G., Ramírez-Aguilar, S.J., Gomez-Porras, J.L., González, W., Thibaud, J.-B., van Dongen, J.T., Dreyer, I., 2011. Potassium (K^+) gradients serve as a mobile energy source in plant vascular tissues. Proc. Natl. Acad. Sci. Unit. States Am. 108 (2), 864–869.

Garcia, D., Gerald, J.N.F., Berger, F., 2005. Maternal control of integument cell elongation and zygotic control of endosperm growth are coordinated to determine seed size in *Arabidopsis*. Plant Cell 17 (1), 52–60.

Geist, K.S., Strassmann, J.E., Queller, D.C., 2019. Family quarrels in seeds and rapid adaptive evolution in *Arabidopsis*. Proc. Natl. Acad. Sci. U.S.A. 116 (19), 9463–9468.

Groot, E.P., Van Caeseele, L.A., 1993. The development of the aleurone layer in canola (*Brassica napus*). Can. J. Bot. 71 (9), 1193–1201.

Guendel, A., Rolletschek, H., Wagner, S., Muszynska, A., Borisjuk, L., 2018. Micro imaging displays the sucrose landscape within and along its allocation pathways. Plant Physiol. 178 (4), 1448–1460.

Hill, L.M., Morley-Smith, E.R., Rawsthorne, S., 2003. Metabolism of sugars in the endosperm of developing seeds of oilseed rape. Plant Physiol. 131, 228–236.

Ingram, G.C., 2017. Dying to live: cell elimination as a developmental strategy in angiosperm seeds. J. Exp. Bot. 68 (4), 785–796.

Ingram, G.C., 2020. Family plot: the impact of the endosperm and other extra-embryonic seed tissues on angiosperm zygotic embryogenesis. F1000Research 9 (F1000 Faculty Rev), 18.

Kawashima, T., Goldberg, R.B., 2010. The suspensor: not just suspending the embryo. Trends Plant Sci. 15, 23–30.

Keith, K., Krami, M., Dengler, N.G., McCourt, P., 1994. Fusca3: a heterochronic mutation affecting late embryo development in *Arabidopsis*. Plant Cell 6, 589–600.

Khan, D., Ziegler, D., Kalichuk, J., Hoi, V., Hyunh, N., Hajihasani, A., Parkin, I., Robinson, S., Belmonte, M., 2020. Gene expression profiling reveals subgenome dominance during Brassica napus seed development. bioRxiv 2020, 04.29.068189.

Lafon-Placette, C., Köhler, C., 2014. Embryo and endosperm, partners in seed development. Curr. Opin. Plant Biol. 17, 64–69.

Lau, S., Slane, D., Herud, O., Kong, J., Jurgens, G., 2012. Early embryogenesis in flowering plants: setting up the basic body pattern. Annu. Rev. Plant Biol. 63, 483–506.

Li, J., Berger, F., 2012. Endosperm: food for humankind and fodder for scientific discoveries. New Phytol. 195, 290–305.

Lohaus, G., Moellers, C., 2000. Phloem transport of amino acids in two *Brassica napus* L. genotypes and one *B. carinata* genotype in relation to their seed protein content. Planta 211, 833–840.

Lorenz, C., Rolletschek, H., Sunderhaus, S., Braun, H.P., 2014. *B. napus* seed endosperm – metabolism and signaling in a dead end tissue. J. Proteomics 108, 382–426.

Lu, J., Le, Hir R., Gómez-Páez, D.M., Coen, O., Péchoux, C., Jasinski, S., Magnani, E., 2021. The nucellus: between cell elimination and sugar transport. Plant Physiol. 185 (2), 478–490.

Meitzel, T., Radchuk, R., McAdam, E.L., Thormählen, I., Feil, R., Munz, E., Hilo, A., Geigenberger, P., Ross, J.J., Lunn, J.E., Borisjuk, L., 2021. Trehalose 6-phosphate promotes seed filling by activating auxin biosynthesis. New Phytol. 229, 1553–1565.

Melkus, G., Rolletschek, H., Fuchs, J., Radchuk, V., Grafahrend-Belau, E., Sreenivasulu, N., Rutten, T., Weier, D., Heinzel, N., Schreiber, F., Altmann, T., Jakob, P., Borisjuk, L., 2011. Dynamic $^{13}C/^{1}H$ NMR imaging uncovers sugar allocation in the living seed. Plant Biotechnol. J. 9, 1022–1037.

Melkus, G., Rolletschek, H., Radchuk, R., Fuchs, J., Rutten, T., Wobus, U., Altmann, T., Jakob, P., Borisjuk, L., 2009. The metabolic role of legume endosperm: a non-invasive imaging study. Plant Physiol. 151, 1139–1154.

Molina, I., Ohlrogge, J.B., Pollard, M., 2008. Deposition and localization of lipid polyester in developing seeds of *Brassica napus* and *Arabidopsis thaliana*. Plant J. 53, 437–449.

Morley-Smith, E.R., Pike, M.J., Findlay, K., Kockenberger, W., Hill, L.M., Smith, A.M., Rawsthorne, S., 2008. The transport of sugars to developing embryos is not via the bulk endosperm in oilseed rape seeds. Plant Physiol. 147, 2121–2130.

Munz, E., Jakob, P.M., Borisjuk, L., 2016. The potential of nuclear magnetic resonance to track lipids in planta. Biochimie 130, 97–108.

Munz, E., Rolletschek, H., Oeltze-Jafra, S., Fuchs, J., Guendel, A., Neuberger, T., Ortleb, S., Jakob, P.M., Borisjuk, L., 2017. A functional imaging study of germinating oilseed rape seed. New Phytol. 216, 1181–1190.

Ohto, M., Floyd, S.K., Fischer, R.L., Goldberg, R.B., Harada, J.J., 2009. Effects of APETALA2 on embryo, endosperm, and seed coat development determine seed size in *Arabidopsis*. Sex. Plant Reprod. 22 (4), 277–289.

Olsen, O.A., 2020. The modular control of cereal endosperm development. Trends Plant Sci. 25 (3), 279–290.

O'Neill, J.P., Colon, K.T., Jenik, P.D., 2019. The onset of embryo maturation in *Arabidopsis* is determined by its developmental stage and does not depend on endosperm cellularization. Plant J. 99 (2), 286–301.

Padmanaban, S., Czerny, D.D., Levin, K.A., Leydon, A.R., Su, R.T., Maugel, T.K., Zou, Y., Cheung, A.Y., Johnson, M.A., Sze, H., 2017. Transporters involved in pH and K^+ homeostasis affect pollen wall formation, male fertility, and embryo development. J. Exp. Bot. 68 (12), 3165–3178.

Patrick, J.W., Offler, C.E., 2001. Compartmentation of transport and transfer events in developing seeds. J. Exp. Bot. 52, 551–564.
Patrick, J.W., Offler, C.E., 2020. Transfer cells: what regulates the development of their intricate wall labyrinths? New Phytol. 228, 427–444.
Penfield, S., 2017. Seed dormancy and germination. Curr. Biol. 27 (17), R874–R878.
Provart, N.J., Alonso, J., Assmann, S.M., Bergmann, D., Brady, S.M., Brkljacic, J., Browse, J., et al., 2016. 50 years of *Arabidopsis* research: highlights and future directions. New Phytol. 209 (3), 921–944.
Radchuk, V., Tran, V., Radchuk, R., Diaz-Mendoza, M., Weier, D., Fuchs, J., Riewe, D., Hensel, G., Kumlehn, J., Munz, E., Heinzel, N., Rolletschek, H., Martinez, M., Borisjuk, L., 2018. Vacuolar processing enzyme 4 contributes to maternal control of grain size in barley by executing programmed cell death in the pericarp. New Phytol. 218, 1127–1142.
Radchuk, V., Sharma, R., Potokina, E., Radchuk, R., Weier, D., et al., 2019. The highly divergent Jekyll genes, required for sexual reproduction, are lineage specific for the related grass tribes Triticeae and Bromeae. Plant J. 98, 961–974.
Radchuk, V., Tran, V., Hilo, A., Muszynska, A., Gündel, A., Wagner, S., Fuchs, J., Hensel, G., Ortleb, S., Munz, E., Rolletschek, H., Borisjuk, L., 2021. Grain filling in barley relies on developmentally controlled programmed cell death. Commun. Biol. 4, 428.
Rolletschek, H., Grafahrend-Belau, E., Munz, E., Radchuk, V., Kartäusch, R., Tschiersch, H., Melkus, G., Schreiber, F., Jakob, P.M., Borisjuk, L., 2015. Metabolic architecture of the cereal grain and its relevance to maximize carbon use efficiency. Plant Physiol. 169, 1698–1713.
Rolletschek, H., Muszynska, A., Borisjuk, L., 2021. The process of seed maturation is influenced by mechanical constrains. New Phytol. 229, 19–23.
Rolletschek, H., Schwender, J., König, C., Chapman, K.D., Romsdahl, T., Lorenz, C., Braun, H.P., Denolf, P., Van Audenhove, K., Munz, E., Heinzel, N., Ortleb, S., Rutten, T., McCorkle, S., Borysyuk, T., Guendel, A., Shi, H., Auwermeulen, M.V., Bourot, S., Borisjuk, L., 2020. Cellular plasticity in response to suppression of storage proteins in the Brassica napus embryo. Plant Cell 32, 2383–2401.
Schiebold, S., Tschiersch, H., Borisjuk, L., Heinzel, N., Radchuk, R., Rolletschek, H., 2011. A novel procedure for the quantitative analysis of metabolites, storage products and transcripts of laser microdissected seed tissues of *Brassica napus*. Plant Methods 7, 19.
Schwender, J., Hebbelmann, I., Heinzel, N., Hildebrandt, T., Rogers, A., Naik, D., Klapperstück, M., Braun, H.-P., Schreiber, F., Denolf, P., Borisjuk, L., Rolletschek, H., 2015. Quantitative multilevel analysis of central metabolism in developing oilseeds of oilseed rape during *in vitro* culture. Plant Physiol. 168, 828–848.
Stadler, R., Lauterbach, C., Sauer, N., 2005. Cell-to-cell movement of green fluorescent protein reveals post-phloem transport in the outer integument and identifies symplastic domains in *Arabidopsis* seeds and embryos. Plant Physiol. 139, 701–712.
Sturtevant, D., Dueñas, M.E., Lee, Y.J., Chapman, K.D., 2017. Three-dimensional visualization of membrane phospholipid distributions in *Arabidopsis thaliana* seeds: a spatial perspective of molecular heterogeneity. Biochim. Biophys. Acta Mol. Cell Biol. Lipids 1862 (2), 268–281.
Sturtevant, D., Lu, S., Zhou, Z.W., Shen, Y., Wang, S., Song, J.M., Zhong, J., Burks, D.J., Yang, Z.Q., Yang, Q.Y., Cannon, A.E., Herrfurth, C., Feussner, I., Borisjuk, L., Munz, E., Verbeck, G.F., Wang, X., Azad, R.K., Singleton, B., Dyer, J.M., Chen, L.L., Chapman, K.D., Guo, L., 2020. The genome of jojoba (*Simmondsia chinensis*): a taxonomically isolated species that directs wax ester accumulation in its seeds. Sci. Adv. 6 (11), eaay3240.
Tikhenko, N., Alqudah, A.M., Borisjuk, L., Ortleb, S., Rutten, T., Wu, D.D., Nagel, M., Himmelbach, A., Mascher, M., Röder, M., Ganal, M., Sehmisch, S., Houben, A., Börner, A., 2020. DEFECTIVE ENDOSPERM-D1 (Dee-D1) is crucial for endosperm development in hexaploid wheat. Commun. Biol. 3, 791.
Ungru, A., Nowack, M.K., Reymond, M., Shirzadi, R., Kumar, M., Biewers, S., Grini, P.E., Schnittger, A., 2008. Natural variation in the degree of autonomous endosperm formation reveals independence and constraints of embryo growth during seed development in *Arabidopsis thaliana*. Genetics 179 (2), 829–841.
Van Lammeren, A.A.M., Kieft, H., Ma, F., van Veenendaal, W.L.H., 1996. Light microscopical study of endosperm formation in *Brassica napus* L. Acta Soc. Bot. Pol. 65, 267–272.
Van Schadewijk, R., Krug, J.R., Shen, D., et al., 2020. Magnetic resonance microscopy at cellular resolution and localised spectroscopy of *Medicago truncatula* at 22.3 tesla. Sci. Rep. 10, 971.
Verboven, P., Herremans, E., Borisjuk, L., Helfen, L., Ho, Q.T., Tschiersch, H., Fuchs, J., Nicolaï, B.M., Rolletschek, H., 2013. Void space inside the developing seed of *Brassica napus* and the modelling of its function. New Phytol. 199, 936–947.
Wang, S., Yokosho, K., Guo, R., Whelan, J., Ruan, Y.L., Ma, J.F., Shou, H., 2019. The soybean sugar transporter GmSWEET15 mediates sucrose export from endosperm to early embryo. Plant Physiol. 180 (4), 2133–2141.
Weber, H., Borisjuk, L., Wobus, U., 2005. Molecular physiology of legume seed development. Annu. Rev. Plant Biol. 56, 253–279.
Werner, D., Gerlitz, N., Stadler, R., 2011. A dual switch in phloem unloading during ovule development in *Arabidopsis*. Protoplasma 248, 225–235.
Woodfield, H.K., Sturtevant, D., Borisjuk, L., Munz, E., Guschina, I.A., Chapman, K.D., Harwood, J.L., 2017. Spatial and temporal mapping of key lipid species in Brassica napus seeds. Plant Physiol. 173, 1998–2009.
Wu, J., Mohamed, D., Dowhanik, S., Petrella, R., Gregis, V., Li, J., Wu, L., Gazzarrini, S., 2020. Spatiotemporal restriction of FUSCA3 expression by class I BPCs promotes ovule development and coordinates embryo and endosperm growth. Plant Cell 32, 1886–1904.
Xiong, H., Wang, W., Sun, M.-X., 2021. Endosperm development is an autonomously programmed process independent of embryogenesis. Plant Cell 33 (4), 1151–1160.
Ziegler, D.J., Khan, D., Kalichuk, J.L., Becker, M.G., Belmonte, M.F., 2019. Transcriptome landscape of the early *Brassica napus* seed. J. Integr. Plant Biol. 61, 639–650.